nature chemical biology

ARTICLES

https://doi.org/10.1038/s41589-018-0192-3

Metalloprotein switches that display chemical-dependent electron transfer in cells

Joshua T. Atkinson[1], Ian J. Campbell[2], Emily E. Thomas[2], Sheila C. Bonitatibus[3], Sean J. Elliott[3], George N. Bennett[4,5] and Jonathan J. Silberg[4,6]*

Biological electron transfer is challenging to directly regulate using environmental conditions. To enable dynamic, protein-level control over energy flow in metabolic systems for synthetic biology and bioelectronics, we created ferredoxin logic gates that utilize transcriptional and post-translational inputs to control energy flow through a synthetic electron transfer pathway that is required for bacterial growth. These logic gates were created by subjecting a thermostable, plant-type ferredoxin to backbone fission and fusing the resulting fragments to a pair of proteins that self-associate, a pair of proteins whose association is stabilized by a small molecule, and to the termini of a ligand-binding domain. We show that the latter domain insertion design strategy yields an allosteric ferredoxin switch that acquires an oxygen-tolerant [2Fe–2S] cluster and can use different chemicals, including a therapeutic drug and an environmental pollutant, to control the production of a reduced metabolite in *Escherichia coli* and cell lysates.

Achieving direct, dynamic control over biological electron transfer (ET) through synthetic biology is critical for creating living sensors and bioelectronics[1–4], controlling microbial electrosynthesis and electrofermentation[5], and building efficient metabolic pathways for chemical synthesis[6,7]. At the hub of mediating the transfer of low-potential electrons is the ferredoxin (Fd) family, ancient iron–sulfur proteins that are deeply rooted in the tree of life[8,9]. These electron carriers are important for ancient metabolic processes, such as hydrogen-dependent CO_2 fixation by autotrophs (acetogens and methanogens) and light-dependent CO_2 fixation by photoautotrophs[10]. Additionally, Fds are widespread across all three domains of life. Some organisms contain over a dozen Fd paralogs, and Fds have been found to support ET to over eighty classes of oxidoreductases[11], suggesting that these electron carriers helped spur the evolution of diverse bioenergetics strategies[12]. Recently, Fds have been used to construct synthetic ET chains. These pathways have been developed to evolve Fd-dependent enzymes with improved catalytic functions[13] and to understand Fd partner specificity[14]. These efforts have demonstrated the potential for manipulating protein electron carriers for synthetic biology. However, we still lack Fds whose ET can be switched "on" and "off" in response to specific environmental conditions.

Some organisms use Fds to dynamically control ET through post-translational modifications. Upon iron–sulfur cluster oxidation, nitrogenase-protecting Fds alter their conformation and binding affinity to nitrogenase to protect from oxidative damage[15,16]. Phosphorylated and calcium-bound forms of Fds were recently discovered in cyanobacteria[17] and rhizobia[18], respectively. These discoveries suggest that Fd ET may also be dynamically regulated through signaling cascades, although the exact mechanisms by which these modifications affect Fd ET remain unclear. Additionally, protein design efforts have investigated whether Fd ET can be deliberately controlled. Fds have been rationally mutated using structural information[19] and have been fused to acceptor proteins to tune the relative proportions of electrons transferred to different metabolic pathways[20–22]. Although these efforts have shown how protein evolution can redirect energy flow, they have yet to yield insight into the ways that Fds acquire new allosteric functions.

Previous studies have shown that proteins can be fragmented into polypeptides whose stable association and cooperative activities are dependent upon ligand-binding events[23]. This has been achieved by fusing engineered fragments to pairs of proteins whose association is stabilized by ligand binding[24,25] and by fusing protein fragments to the termini of ligand-binding domains[25,26]. To investigate whether a similar design approach could be used to create protein electron carriers that are regulated by environmental conditions, we rationally designed four split Fds (sFds) and evaluated their ability to support ET in cells. All four sFds supported ET in cells when they were fused to peptides that stabilize fragment association, and three of the sFds could be used as transcriptional AND gates in which a pair of conditional promoters regulate Fd-mediated ET. One of the sFds could also be used to create a three-hybrid system that only supports cellular ET transfer when both fragments are expressed and cells are exposed to the small molecule rapamycin. Additionally, when the fragments of this sFd were fused to the termini of the estrogen receptor (ER) ligand-binding domain (LBD), the resulting polypeptide presented ET that could be enhanced post-translationally by different estrogen-receptor modulators.

Results

Monitoring protein electron transfer using a selection. To rapidly assay ET mediated by engineered Fds, we used *E. coli* EW11 (ref. [13]), a strain that cannot grow in minimal medium containing sulfate as a sulfur source unless it expresses a synthetic ET chain consisting of a Fd-$NADP^+$ reductase (FNR) electron donor, a Fd electron carrier, and a Fd-dependent sulfite reductase (SIR) electron acceptor (Fig. 1a). Endogenous oxidoreductases were systematically removed from the genome of this strain to insulate Fd-dependent redox

[1]Systems, Synthetic, and Physical Biology Graduate Program, Rice University, Houston, TX, USA. [2]Biochemistry and Cell Biology Graduate Program, Rice University, Houston, TX, USA. [3]Department of Chemistry, Boston University, Boston, MA, USA. [4]Department of BioSciences, Rice University, Houston, TX, USA. [5]Department of Chemical and Biomolecular Engineering, Rice University, Houston, TX, USA. [6]Department of Bioengineering, Rice University, Houston, TX, USA. *e-mail: joff@rice.edu

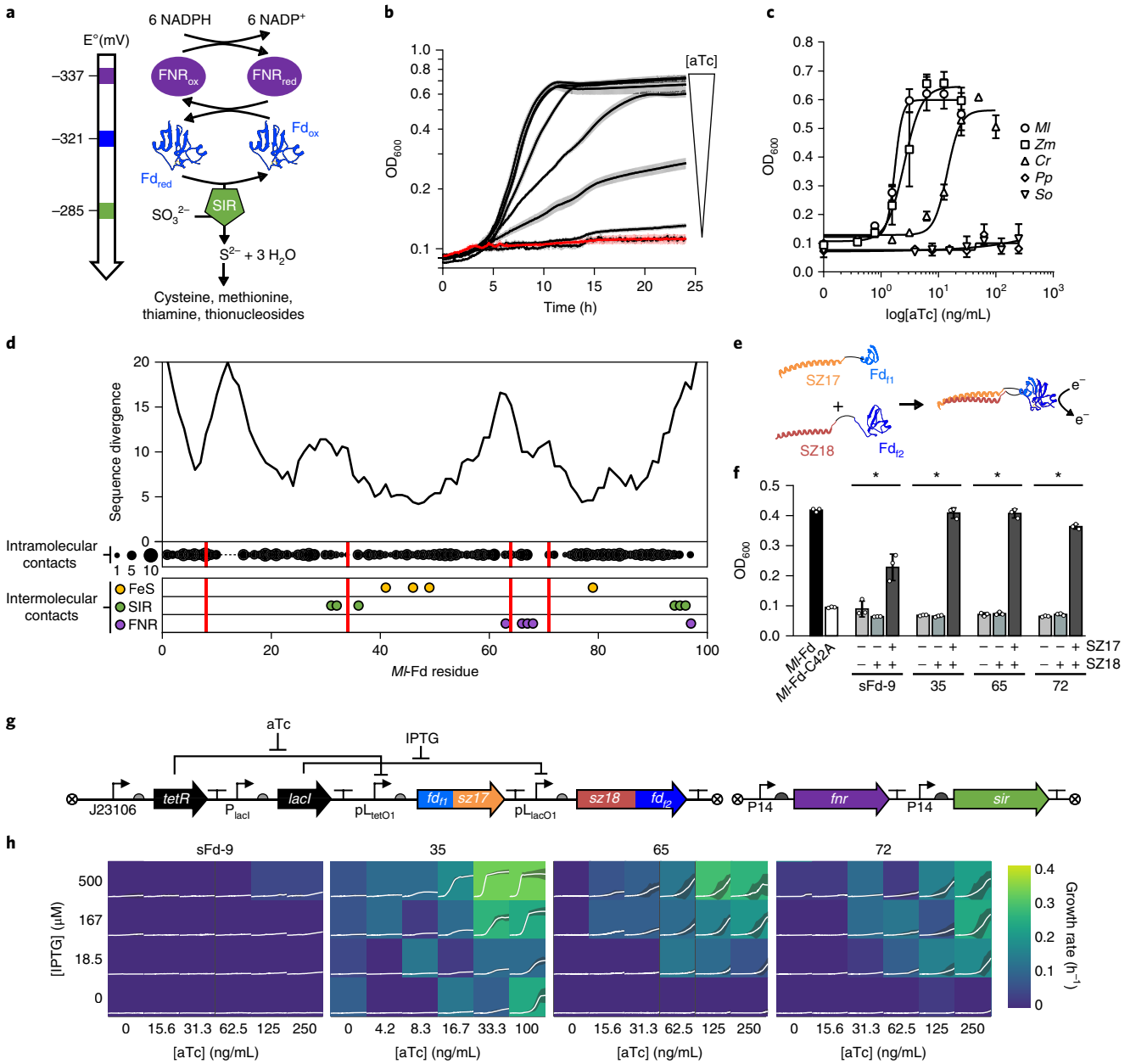

Fig. 1 | Designing split Fds that transfer electrons within cells. a, A synthetic ET pathway coupling NADPH oxidation by FNR to sulfide production by SIR using Fd-mediated ET. **b**, The effect of varying concentrations of aTc (0.4, 0.8, 1.6, 3.1, 6.3, 12.5, and 25 ng/mL) on the growth of cells expressing *MI*-Fd from an aTc-inducible P_{LtetO1} promoter and FNR and SIR from constitutive promoters. The red line represents the mean in the absence of aTc, black lines represents the mean in the presence of aTc, and the error bars represent the s.d. ($n = 3$ biologically independent samples). **c**, Growth complementation observed after 24 h with *Mastigocladus laminosus* (*MI*; $k_{1/2} = 1.8$ ng/mL aTc), *Zea mays* root (*Zm*; $k_{1/2} = 2.5$ ng/mL aTc), *Chlamydomonas reinhardtii* (*Cr*; $k_{1/2} = 14.2$ ng/mL aTc), *Spinacia oleracea* (*So*; $k_{1/2} > 250$ ng/mL), and *Prochlorococcus* phage P-SSM2 (*Pp*; $k_{1/2} > 250$ ng/mL) Fds. Symbols and error bars represent the mean and s.d., respectively ($n = 3$ biologically independent samples). **d**, The number of different amino acids observed at each residue position within a Fd multiple sequence alignment mapped onto the *MI*-Fd primary structure (top). The backbone fission sites used to generate sFds (red lines) are compared to the number of intramolecular residue–residue contacts ($n = 0$ to 10, displayed as proportionally sized black circles) within the structure of *MI*-Fd (PDB: 1RFK), as well as intermolecular binding residues, including the cysteines that coordinate the [2Fe-2S] cluster (yellow) and the residues that contact SIR[29] (green) and FNR[30] (purple). **e**, Each pair of sFd fragments, Fd_{f1} and Fd_{f2} (blue), was expressed as a fusion to SYNZIP-17 (SZ17; orange) and SYNZIP-18 (SZ18; red), respectively. **f**, Complementation of *E. coli* EW11 growth by *MI*-Fd and a C42A mutant of *MI*-Fd lacking a cysteine required for coordinating iron is compared to the complementation observed in cells expressing Fd_{f1} and Fd_{f2} alone, Fd_{f1} and the SZ18-Fd_{f2} fusion, and Fd_{f1} and Fd_{f2} fused to SZ17 and SZ18, respectively. Bars and error bars represent the average and s.d., respectively ($n = 3$ biologically independent samples). Significant growth relative to the C42A mutant is shown by an asterisk (sFd-9: $^*P = 2 \times 10^{-3}$; sFd-35: $^*P = 8 \times 10^{-4}$; sFd-65: $^*P = 6 \times 10^{-4}$; sFd-72: $^*P = 1 \times 10^{-4}$, using a two-tailed, independent *t*-test). **g**, The genetic circuit used to regulate Fd fragment expression. The Fd_{f1}-S17 fusion is expressed using an aTc-inducible promoter, the S18-Fd_{f2} fusion is expressed using an IPTG-inducible promoter, and the partner proteins are constitutively expressed. **h**, Effects of sFd fragment concentration, controlled by aTc and IPTG, on *E. coli* EW11 complementation. Each box shows the cell density from cultures, with the growth rate (h^{-1}) indicated by the color. The white lines and shaded region within each box represent the cell density mean and s.d., respectively ($n = 3$ biologically independent samples).

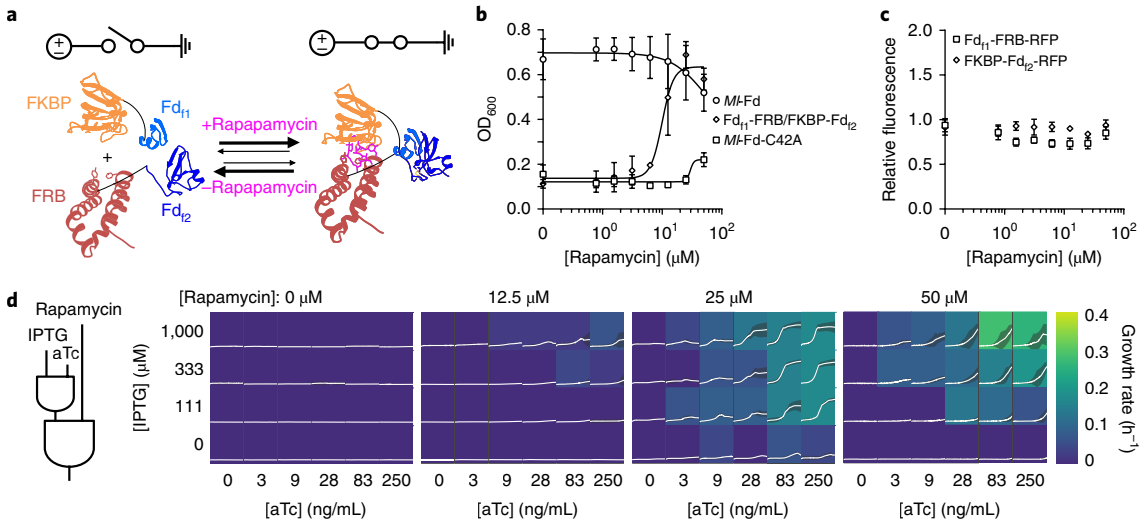

Fig. 2 | Post-translational control over Fd electron transfer in cells. a, sFd-35 fragments Fd$_{f1}$ and Fd$_{f2}$ (blue) were expressed as fusions to FKBP (orange) and FRB (red), respectively. **b**, Effect of rapamycin concentration on *E. coli* EW11 growth in the presence of aTc (150 ng/mL) and IPTG (500 μM) concentrations that yielded strong complementation with SZ17/SZ18 fusions. Complementation by Fd$_{f1}$-FRB/FKBP-Fd$_{f2}$ ($k_{1/2}$ = 9.95 μM rapamycin) is compared to that of *Ml*-Fd and a C42A mutant of *Ml*-Fd that lacks a cysteine required for coordinating iron. Growth of cells expressing Fd$_{f1}$-FRB/FKBP-Fd$_{f2}$ is enhanced significantly compared to the C42A mutant when ≥25 μM rapamycin is added (25 μM: $P = 1 \times 10^{-4}$; 50 μM: $P = 6 \times 10^{-5}$; two-tailed, independent *t*-test). Symbols and error bars represent the mean and s.d., respectively ($n = 3$ biologically independent samples). **c**, The effect of rapamycin on the relative fluorescence of cells expressing Fd$_{f1}$-FKBP-RFP and FRB-Fd$_{f2}$-RFP. Upon addition of rapamycin in ethanol, there was no significant increase in fluorescence for either fragment compared to ethanol alone ($P > 0.01$ using a two-tailed, independent *t*-test). Symbols and error bars represent the mean and s.d., respectively ($n = 3$ biologically independent samples). All fluorescent reporters were appended to the C terminus of proteins to maintain the context of the ribosomal binding sites and translation initiation[44]. **d**, Fd$_{f1}$-FRB and FKBP-Fd$_{f2}$ can function as a three-input AND gate that uses aTc, IPTG, and rapamycin to control electron flow. Each box shows cell density from cultures, with the growth rate (h^{-1}) indicated by the color. The white lines and shaded region within each box represent the cell density mean and s.d., respectively ($n = 3$ biologically independent samples).

pathways from native redox reactions[13]. To evaluate Fd ET in cells, we constitutively expressed *Zea mays* FNR and SIR and used a TetR-repressible promoter to control the expression of plant-type [2Fe-2S] Fds. With this expression strategy, growth depended upon the level of anhydrotetracycline (aTc) (Fig. 1b), and thus the amount of Fd available to mediate ET.

We analyzed the effect of aTc on complementation by five [2Fe–2S] Fds, including plant, cyanobacterial, algal, and phage family members (Fig. 1c). Two of the Fds were unable to complement growth, including *Spinacia oleracea* and *Prochlorococcus* phage P-SSM2 Fds. The other three Fds presented half-maximal concentrations at different aTc concentrations. *Mastigocladus laminosus* Fd (*Ml*-Fd) yielded half-maximal complementation at the lowest aTc concentration. This thermostable Fd, which displays optimal ET at 65 °C[27], was targeted for all subsequent design efforts to minimize the destabilizing effects of mutations, as previous studies have shown that tolerance to fission correlates with thermostability[28].

Design of split protein electron carriers. To identify backbone fission locations that are nondisruptive to the *Ml*-Fd structure, we generated a multiple sequence alignment of [2Fe–2S] Fds (Supplementary Fig. 1) and calculated the number of different amino acids at each native *Ml*-Fd position (Fig. 1d). We targeted four sites with moderate sequence divergence for backbone fission, including the peptide bonds following residues 9, 35, 65, and 72. We chose these sites because they vary in their distances from the [2Fe–2S] cluster, and they differ in the number of cofactor and partner-binding residues encoded distributed across the pair of fragments.

In the *Ml*-Fd structure[27], the backbone cleavage sites occur 9.5 to 18.5 Å from the [2Fe–2S] cluster (Supplementary Fig. 2). For two of the sFd proteins, sFd-9 and sFd-35, all of the cysteines that coordinate iron reside on a single polypeptide (Fig. 1d). The other split proteins, sFd-65 and sFd-72, have their iron-coordinating cysteines dispersed across the fragments, potentially requiring [2Fe–2S] cluster maturation following fragment complementation. Mapping the backbone fission sites onto the Fd–SIR complex structure[29] revealed that the SIR-contacting residues in these sFds are divided among the different polypeptide fragments in sFd-35, sFd-65, and sFd-72 (Supplementary Fig. 3). By contrast, the FNR-contacting residues in the Fd–FNR complex[30] are only divided among the different fragments in sFd-65 and sFd-72.

Split ferredoxins support electron transfer in cells. To assist with sFd ET, each pair of Fd fragments was initially expressed as a fusion to SYNZIP-17 and SYNZIP-18 (Fig. 1e), synthetic peptides that stably associate to form a coiled coil[31]. When the sFds were expressed in *E. coli* EW11, complementation was observed with all four variants (Fig. 1f), albeit to varying extents. Removal of one or both SYNZIP peptides abolished growth in all cases, suggesting that these split proteins uniformly require assistance with fragment association for efficient ET. TetR- and LacI-repressible promoters were also used to control the expression of each Fd–fragment fusion (Fig. 1g), and complementation was analyzed over a range of aTc and isopropyl β-D-1-thiogalactopyranoside (IPTG) concentrations (Fig. 1h). sFd-35, sFd-65, and sFd-72 all functioned as two-input AND gates to control the production of a reduced sulfur metabolite, with sFd-35 exhibiting the highest tunable range. In the case of sFd-35, a low level of complementation was observed when cells were exposed to aTc in the absence of IPTG. This finding is thought to arise as a consequence of leaky expression of the C-terminal Fd fragment.

To investigate whether sFd ET can be regulated post-translationally, we created vectors for expressing the three most active split proteins as fusions to FKBP12 and the FKBP-rapamycin binding (FRB) domain of mTOR (Fig. 2a), proteins whose interaction is stabilized by rapamycin[32], and we assessed their complementation of *E. coli* EW11 growth in the presence and absence of rapamycin.

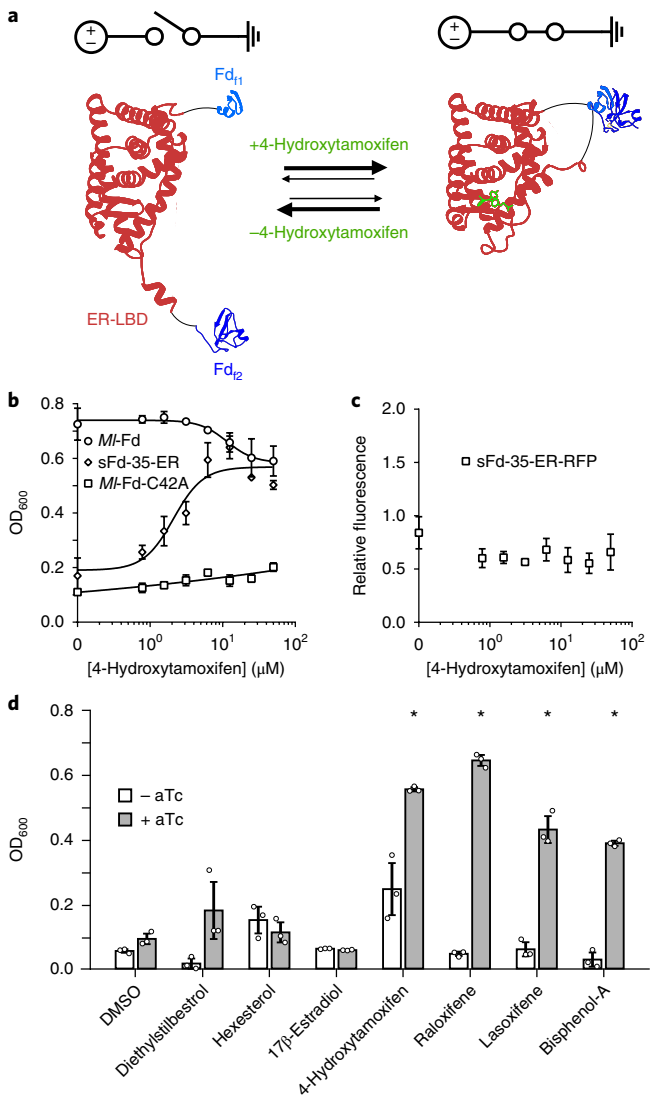

Fig. 3 | Using domain insertion to create a Fd switch. a, The ER-LBD was inserted after residue 35 in *Ml*-Fd to create sFd-35-ER. **b**, Effect of 4-hydroxytamoxifen (4-HT) concentration on the complementation of *E. coli* EW11 by sFd-35-ER ($k_{1/2}$ = 2.11 μM 4-HT), *Ml*-Fd, and *Ml*-Fd-C42A. Growth of sFd-35-ER is enhanced significantly compared to the C42A mutant in the presence of ≥6.25 μM 4-HT (6.25 μM: $P = 6\times10^{-3}$; 12.5 μM: $P = 4\times10^{-4}$; 25 μM: $P = 1\times10^{-4}$; 50 μM: $P = 2\times10^{-5}$; two-tailed, independent *t*-test). Symbols and error bars represent the mean and s.d., respectively ($n = 3$ biologically independent samples). **c**, The effect of 4-HT on the relative fluorescence of cells expressing sFd-35-ER-RFP. Upon addition of 4-HT in ethanol, there was no significant increase in fluorescence compared to ethanol alone ($P > 0.01$ using a two-tailed, independent *t*-test). Symbols and error bars represent the mean and s.d., respectively ($n = 3$ biologically independent samples). All fluorescent reporters were amended to the C terminus of proteins to maintain the context of the ribosomal binding sites and translation initiation[44]. **d**, Effect of estrogen receptor modulators (50 μM) on complementation of *E. coli* EW11 by sFd-35-ER with 0 ng/mL aTc (white bars) or 200 ng/mL aTc (gray bars). The agonists (diethylstilbestrol, hexestrol, and 17β-estradiol) do not significantly enhance growth of EW11 cells compared to DMSO alone ($P > 0.01$ using a two-tailed, independent *t*-test), whereas the antagonists (4-hydroxytamoxifen, raloxifene, and lasoxifene) as well as bisphenol-A significantly enhance growth compared to DMSO alone. * represents significant growth (4-hydroxytamoxifen: $P = 1\times10^{-4}$; raloxifene: $P = 5\times10^{-6}$; lasoxifene: $P = 3\times10^{-3}$; bisphenol-A: $P = 2\times10^{-4}$; two-tailed, independent *t*-test). Bars and error bars represent the average and s.d., respectively ($n = 3$ biologically independent samples).

These sFds were expressed using TetR- and LacI-repressible promoters (Supplementary Fig. 4a), and complementation was measured using inducer concentrations that yielded maximal growth when sFds were fused to SYNZIP peptides. In the absence of rapamycin, none of the sFds complemented growth. Addition of rapamycin enhanced the growth of cells expressing sFd-35 (Fig. 2b), but not sFd-65 and sFd-72 (Supplementary Fig. 5). In cases with sFd-35, growth was dose dependent and could be tuned to a maximal density similar to those in cells expressing *Ml*-Fd.

To evaluate whether rapamycin affected sFd-35 expression, we examined rapamycin effects on protein accumulation using fragments fused to red fluorescent protein (RFP). With each sFd fragment, this analysis revealed similar RFP levels in the presence and absence of rapamycin (Fig. 2c). These findings provide evidence that ET is controlled post-translationally by rapamycin stabilization of the sFd fragment complex. Complementation measurements performed using different combinations of aTc, IPTG, and rapamycin revealed that sFd-35 can be used as a three-input AND gate to control ET for sulfide production and growth (Fig. 2d).

A ferredoxin switch created using domain insertion. Allosteric protein switches have been engineered by fusing protein fragments to the termini of domains that undergo chemical-dependent conformational changes[25,26]. To test whether this domain-insertion strategy can be used to diversify the chemical regulation of *Ml*-Fd, we inserted the ligand-binding domain (LBD) of the human estrogen receptor (ER) after residue 35 to create sFd-35-ER (Fig. 3a). This LBD was chosen because it undergoes a conformational change upon binding of 4-hydroxytamoxifen (4-HT) that alters the proximity of the protein termini[33]. In addition, we recently found that insertion of the ER-LBD into an aminoacyl-tRNA synthetase yields protein switches with 4-HT-dependent activities[25].

We evaluated the activity of sFd-35-ER by expressing this protein using an aTc-inducible promoter (Supplementary Fig. 4b). In medium containing aTc, sFd-35-ER did not significantly enhance *E. coli* EW11 growth following a 48-h incubation (Fig. 3b). By contrast, complementation was enhanced to *Ml*-Fd levels when cells were grown in the presence of aTc and 4-HT. We also expressed this protein as a fusion to RFP (sFd-35-ER-RFP) to evaluate how 4-HT affects protein expression. This analysis revealed similar expression across a range of 4-HT concentrations (Fig. 3c), providing evidence that the increased complementation arises from 4-HT effects on sFd-35-ER ET rather than increases in expression.

The ER-LBD binds two classes of estrogen-receptor modulators, agonists and antagonists, which elicit distinct conformations (Supplementary Fig. 6) and tissue-specific responses in vivo[33,34]. To evaluate how these different modulators affect sFd-35-ER ET, we evaluated sFd-35-ER growth complementation in the presence of agonists, antagonists, and an endocrine disruptor (Fig. 3d). This analysis revealed that sFd-35-ER ET is chemically selective and is activated by the ER antagonists (4-HT and raloxifene, lasoxifene) and endocrine disruptor (bisphenol-A). However, this switch is not activated by the ER agonists (17β-estradiol, diethylstilbestrol, and hexestrol).

In vitro characterization of the ferredoxin switch. To understand how *Ml*-Fd iron–sulfur cluster binding and ET are affected by domain insertion, sFd-35-ER was overexpressed in *E. coli* and purified under aerobic conditions. Recombinant sFd-35-ER was brown in color throughout the purification protocol (Supplementary Fig. 7) and presented absorbance (Fig. 4a) and visible circular dichroism (CD) spectra (Fig. 4b) that were consistent with the presence of a [2Fe–2S] metallocluster and similar to those in *Ml*-Fd and other plant-type Fds[35,36].

To investigate whether domain insertion affects the reduction potential of *Ml*-Fd, we characterized *Ml*-Fd and sFd-35-ER using protein film voltammetry[37]. In the absence of 4-HT, we found that

the midpoint potentials of *Ml*-Fd and sFd-35-ER (Fig. 4c) were −336 and −320 mV, respectively. These measurements indicate that sFd-35-ER retains a potential that is adequate for coupling NADPH oxidation by FNR (FAD E° = −337 mV)[38] to sulfite reduction by SIR ([4Fe–4S] E° = −415 mV, siroheme = −285 mV)[39]. In the presence of 4-HT, *Ml*-Fd presented a similar midpoint potential (−330 mV) to that in the absence of ligand, whereas sFd-35-ER yielded a +27 mV shift in potential (−293 mV). These findings provide evidence that domain insertion can be used to create a Fd whose redox potential is tuned by chemical binding, and suggest that this design approach could be applied to proteins with alternative [2Fe–2S] cluster ligands to create switches capable of regulating ET over a range of potentials[11,40].

To directly demonstrate that purified sFd-35-ER functions as a switch in vitro, we examined whether this protein could support sulfide production in lysates derived from *E. coli* EW11 expressing only FNR and SIR (Fig. 4d). We monitored SIR activity in desalted cell lysates using sulfidefluor-7 (SF7)[41], a fluorescent probe for hydrogen sulfide. Cell extracts derived from *E. coli* EW11 expressing FNR and SIR presented sulfide production rates that depended upon NADPH concentration (Supplementary Fig. 8). To minimize this background signal, we added a low level of NADPH (40 μM) that did not yield large sulfide production rates over the time course of our measurements. In this in vitro assay, the rate of sulfide production is proportional to the concentration of *Ml*-Fd added to cell lysates (Supplementary Fig. 9). The sulfide production rate was not enhanced by adding 4-HT alone, demonstrating that this chemical does not support ET to SIR in the absence of a Fd. Addition of purified sFd-35-ER to cell lysates containing FNR and SIR increased the sulfide production rate (Fig. 4e), indicating that this protein can mediate ET to SIR in the absence of 4-HT. However, in the presence of 4-HT, the sulfide production rate was significantly enhanced. Taken together, these measurements provide direct evidence that 4-HT regulates sulfide production by altering the conformation of sFd-35-ER and the efficiency with which it transfers electrons from FNR to SIR.

Discussion

Chemical-dependent protein electron carriers represent a new class of synthetic switches that will enable precision control over electron flow in cells. Herein, we show that these electrical switches can be used to control ET from FNR to SIR. These electron donor and acceptor proteins were used as partner proteins because they allowed the rapid assessment of Fd-mediated ET using growth complementation of a nutritional requirement. Previous studies have shown that Fds can support ET in diverse non-native pathways, such as hydrogen[13,19,20], propane[7], and antibiotic synthesis[6]. These observations suggest that our chemical-dependent Fds could be used to regulate diverse metabolic outputs by expressing them in parallel with FNR and alternative electron acceptors that are also dependent on [2Fe–2S] Fds, such as aldehyde decarbonylase[7], cytochrome P450 (ref. [22]), and glutamine oxoglutarate aminotransferase[42].

A thermostable Fd was used a starting point for switch design to maximize the likelihood of discovering Fd variants capable of ET. Among the different backbone fission sites tested, cleavage after residue 35 yielded the most robust fragments for different design strategies. With this sFd, ET was enhanced by fusion to SYNZIP-17/18 or fusion to FKBP/FRB; the other sFds were only functional when fused to the SYNZIP peptides. Additionally, sFd-35 fragments could be fused to the ends of the ER LBD to create a chemical-dependent Fd. These findings suggest that structurally related fragments in other [2Fe–2S] Fds could be used to create similar protein switches. By applying this design strategy to Fds with distinct partner specificities from *Ml*-Fd, Fds could be created that extend the diversity of metabolic outputs that can be regulated using ER antagonists at the level of ET.

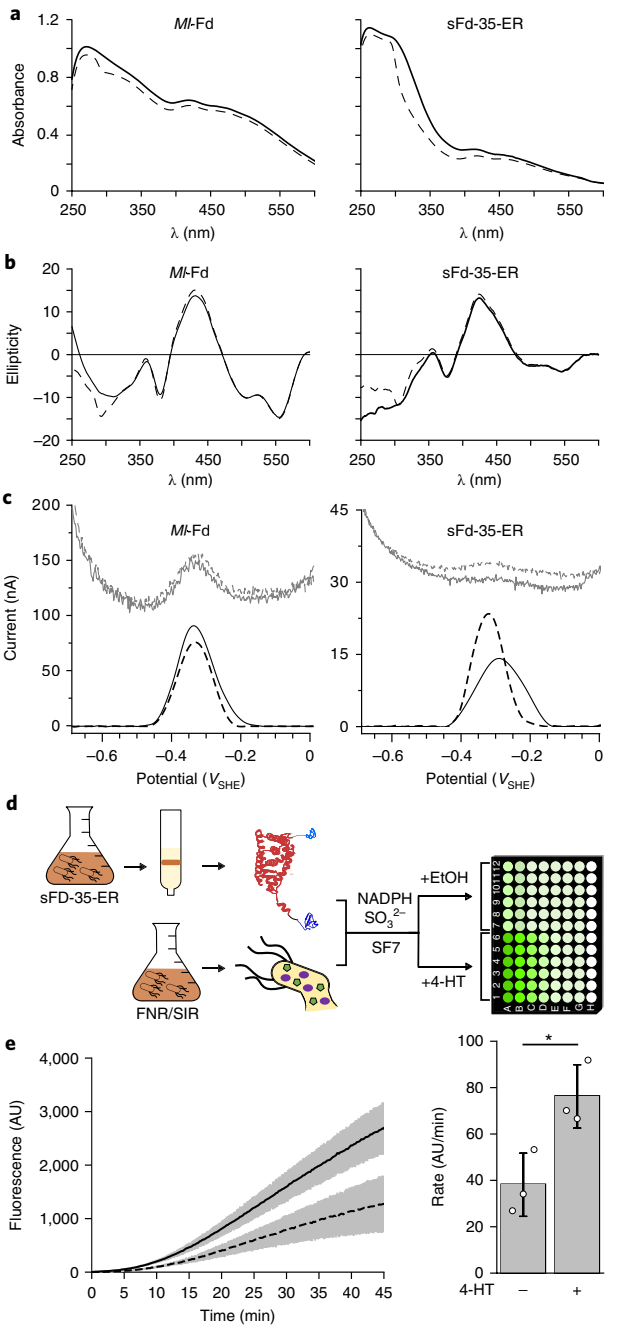

Fig. 4 | Using purified sFd-35-ER to control metabolite production in cell lysates. a,**b**, The absorbance (**a**) and circular dichroism (**b**) spectra of purified sFd-35-ER and *Ml*-Fd (150 μM each) in the presence (solid line) or absence (dashed line) of 4-HT display features characteristic of [2Fe–2S] proteins[36]. **c**, The midpoint potentials of *Ml*-Fd and sFd-35-ER in the presence (solid line) or absence (dashed line) of 4-HT. Raw square wave voltammetry data are plotted in gray, and baseline-subtracted data are plotted in black. Experiments depicted in **a**–**c** were performed twice using two independent protein preparations and yielded the same results. **d**, Lysates generated from *E. coli* EW11 constitutively expressing FNR and SIR were mixed with purified sFd-35-ER (50 nM), NADPH (40 μM), SO_3^{2-} (10 mM), and SF7 (2 μM). Following mixing, 4-HT in ethanol (solid line) or an equivalent amount of ethanol (dashed line) were added to reactions, and fluorescence was monitored at 37 °C. **e**, The sFd-35-ER switch displayed a significant increase in sulfide production rate upon addition of 4-HT ($P = 0.027$, using a two-tailed, independent *t*-test) relative to the ethanol carrier. The black lines and bars represent the mean, and the gray shaded region and error bars represent the s.d. ($n = 3$ independent experiments).

Fd switches with [2Fe–2S] clusters should be useful for regulating ET across the range of midpoint potentials where native Fds function (−455 to −262 mV)[11]. To create switches that support ET at more negative potentials, our design approach could be applied to clostridial-type Fds, which possess multiple [4Fe–4S] clusters[11,40]. Modern clostridial Fds are thought to have arisen from duplication of smaller peptides that required association to function[8]. These smaller peptides have been synthesized and have been shown to coordinate iron–sulfur clusters in vitro[43], suggesting that they may be capable of supporting ET from FNR to SIR when expressed in cells. Additionally, our design approach could be applied to families of protein electron carriers that support ET at more positive midpoint potentials, such as cytochromes, thioredoxins, Rieske-type Fds, and cupredoxins[11]. The major challenge with applying this design strategy to other protein electron carriers will be the development of high-throughput assays that can be used to rapidly mine combinatorial libraries of engineered proteins for variants that display chemical-dependent ET.

Electrical protein switches have a potentially wide range of applications in bioelectronics, metabolic engineering, and synthetic biology. They can be used in place of native oxidoreductases to regulate the flow of electrons derived from oxidative metabolism and photosynthesis in response to specific metabolic or environmental cues. They can also be used to dynamically regulate electron flow between central metabolism and non-native metabolic pathways[6,7,13,19,20]. Furthermore, electrical protein switches can be used to couple the exquisite sensing capabilities of proteins to electrical communication between cells and conductive materials outside of cells[1]. To date, electron conduits have been described whose extracellular ET can be tuned using transcriptional regulation[2–4]. By coupling exoelectrogen current production to electrical protein switches, post-translational control over cellular current production may be possible that does not require slow transcriptional and translational processes. In the future, the ligand specificity of these switches could be diversified by fusing Fd fragments to different ligand-binding domains and by mutating the ligand-binding site of our prototype switches.

Online content

Any methods, additional references, Nature Research reporting summaries, source data, statements of data availability and associated accession codes are available at https://doi.org/10.1038/s41589-018-0192-3.

Received: 17 August 2018; Accepted: 7 November 2018;
Published online: 17 December 2018

References

1. Jensen, H. M. et al. Engineering of a synthetic electron conduit in living cells. *Proc. Natl Acad. Sci. USA* **107**, 19213–19218 (2010).
2. Webster, D. P. et al. An arsenic-specific biosensor with genetically engineered *Shewanella oneidensis* in a bioelectrochemical system. *Biosens. Bioelectron.* **62**, 320–324 (2014).
3. Golitsch, F., Bücking, C. & Gescher, J. Proof of principle for an engineered microbial biosensor based on *Shewanella oneidensis* outer membrane protein complexes. *Biosens. Bioelectron.* **47**, 285–291 (2013).
4. West, E. A., Jain, A. & Gralnick, J. A. Engineering a native inducible expression system in *Shewanella oneidensis* to control extracellular electron transfer. *ACS Synth. Biol.* **6**, 1627–1634 (2017).
5. Kracke, F., Vassilev, I. & Krömer, J. O. Microbial electron transport and energy conservation - the foundation for optimizing bioelectrochemical systems. *Front. Microbiol.* **6**, 575 (2015).
6. Shomar, H. et al. Metabolic engineering of a carbapenem antibiotic synthesis pathway in *Escherichia coli*. *Nat. Chem. Biol.* **14**, 794–800 (2018).
7. Kallio, P., Pásztor, A., Thiel, K., Akhtar, M. K. & Jones, P. R. An engineered pathway for the biosynthesis of renewable propane. *Nat. Commun.* **5**, 4731 (2014).
8. Eck, R. V. & Dayhoff, M. O. Evolution of the structure of ferredoxin based on living relics of primitive amino acid sequences. *Science* **152**, 363–366 (1966).
9. Harel, A., Bromberg, Y., Falkowski, P. G. & Bhattacharya, D. Evolutionary history of redox metal-binding domains across the tree of life. *Proc. Natl Acad. Sci. USA* **111**, 7042–7047 (2014).
10. Sousa, F. L. et al. Early bioenergetic evolution. *Phil. Trans. R. Soc. Lond. B* **368**, 20130088 (2013).
11. Atkinson, J. T., Campbell, I., Bennett, G. N. & Silberg, J. J. Cellular assays for ferredoxins: a strategy for understanding electron flow through protein carriers that link metabolic pathways. *Biochemistry* **55**, 7047–7064 (2016).
12. Hall, D. O., Cammack, R. & Rao, K. K. Role for ferredoxins in the origin of life and biological evolution. *Nature* **233**, 136–138 (1971).
13. Barstow, B. et al. A synthetic system links FeFe-hydrogenases to essential *E. coli* sulfur metabolism. *J. Biol. Eng.* **5**, 7 (2011).
14. Yang, J., Xie, X., Yang, M., Dixon, R. & Wang, Y.-P. Modular electron-transport chains from eukaryotic organelles function to support nitrogenase activity. *Proc. Natl Acad. Sci. USA* **114**, E2460–E2465 (2017).
15. Schlesier, J., Rohde, M., Gerhardt, S. & Einsle, O. A conformational switch triggers nitrogenase protection from oxygen damage by shethna protein II (FeSII). *J. Am. Chem. Soc.* **138**, 239–247 (2016).
16. Milton, R. D. et al. The in vivo potential-regulated protective protein of nitrogenase in *Azotobacter vinelandii* supports eerobic bioelectrochemical dinitrogen reduction in vitro. *J. Am. Chem. Soc.* **139**, 9044–9052 (2017).
17. Angeleri, M., Zorina, A., Aro, E.-M. & Battchikova, N. Interplay of SpkG kinase and the Slr0151 protein in the phosphorylation of ferredoxin 5 in *Synechocystis* sp. strain PCC 6803. *FEBS Lett.* **592**, 411–421 (2018).
18. Moscatiello, R. et al. Identification of ferredoxin II as a major calcium binding protein in the nitrogen-fixing symbiotic bacterium *Mesorhizobium loti*. *BMC. Microbiol.* **15**, 16 (2015).
19. Rumpel, S. et al. Enhancing hydrogen production of microalgae by redirecting electrons from photosystem I to hydrogenase. *Energy Environ. Sci.* **7**, 3296–3301 (2014).
20. Eilenberg, H. et al. The dual effect of a ferredoxin-hydrogenase fusion protein in vivo: successful divergence of the photosynthetic electron flux towards hydrogen production and elevated oxygen tolerance. *Biotechnol. Biofuels.* **9**, 182 (2016).
21. Yacoby, I. et al. Photosynthetic electron partitioning between [FeFe]-hydrogenase and ferredoxin:NADP$^+$-oxidoreductase (FNR) enzymes in vitro. *Proc. Natl Acad. Sci. USA* **108**, 9396–9401 (2011).
22. Mellor, S. B. et al. Fusion of ferredoxin and cytochrome P450 enables direct light-driven biosynthesis. *ACS. Chem. Biol.* **11**, 1862–1869 (2016).
23. Stein, V. & Alexandrov, K. Synthetic protein switches: design principles and applications. *Trends Biotechnol.* **33**, 101–110 (2015).
24. Pelletier, J. N., Campbell-Valois, F. X. & Michnick, S. W. Oligomerization domain-directed reassembly of active dihydrofolate reductase from rationally designed fragments. *Proc. Natl Acad. Sci. USA* **95**, 12141–12146 (1998).
25. Thomas, E. E., Pandey, N., Knudsen, S., Ball, Z. T. & Silberg, J. J. Programming post-translational control over the metabolic labeling of cellular proteins with a noncanonical amino acid. *ACS Synth. Biol.* **6**, 1572–1583 (2017).
26. Guntas, G., Mansell, T. J., Kim, J. R. & Ostermeier, M. Directed evolution of protein switches and their application to the creation of ligand-binding proteins. *Proc. Natl Acad. Sci. USA* **102**, 11224–11229 (2005).
27. Fish, A., Danieli, T., Ohad, I., Nechushtai, R. & Livnah, O. Structural basis for the thermostability of ferredoxin from the cyanobacterium *Mastigocladus laminosus*. *J. Mol. Biol.* **350**, 599–608 (2005).
28. Segall-Shapiro, T. H. et al. Mesophilic and hyperthermophilic adenylate kinases differ in their tolerance to random fragmentation. *J. Mol. Biol.* **406**, 135–148 (2011).
29. Kim, J. Y., Nakayama, M., Toyota, H., Kurisu, G. & Hase, T. Structural and mutational studies of an electron transfer complex of maize sulfite reductase and ferredoxin. *J. Biochem.* **160**, 101–109 (2016).
30. Kurisu, G. et al. Structure of the electron transfer complex between ferredoxin and ferredoxin-NADP(+) reductase. *Nat. Struct. Biol.* **8**, 117–121 (2001).
31. Reinke, A. W., Grant, R. A. & Keating, A. E. A synthetic coiled-coil interactome provides heterospecific modules for molecular engineering. *J. Am. Chem. Soc.* **132**, 6025–6031 (2010).
32. Michnick, S. W., Rosen, M. K., Wandless, T. J., Karplus, M. & Schreiber, S. L. Solution structure of FKBP, a rotamase enzyme and receptor for FK506 and rapamycin. *Science* **252**, 836–839 (1991).
33. Shiau, A. K. et al. The structural basis of estrogen receptor/coactivator recognition and the antagonism of this interaction by tamoxifen. *Cell* **95**, 927–937 (1998).
34. Paige, L. A. et al. Estrogen receptor (ER) modulators each induce distinct conformational changes in ER alpha and ER beta. *Proc. Natl Acad. Sci. USA* **96**, 3999–4004 (1999).
35. Stephens, P. J. et al. Circular dichroism and magnetic circular dichroism of iron-sulfur proteins. *Biochemistry* **17**, 4770–4778 (1978).
36. Ta, D. T. & Vickery, L. E. Cloning, sequencing, and overexpression of a [2Fe-2S] ferredoxin gene from *Escherichia coli*. *J. Biol. Chem.* **267**, 11120–11125 (1992).

37. Bak, D. W., Zuris, J. A., Paddock, M. L., Jennings, P. A. & Elliott, S. J. Redox characterization of the FeS protein MitoNEET and impact of thiazolidinedione drug binding. *Biochemistry* **48**, 10193–10195 (2009).
38. Aliverti, A. et al. Biochemical and crystallographic characterization of ferredoxin-NADP$^+$ reductase from nonphotosynthetic tissues. *Biochemistry* **40**, 14501–14508 (2001).
39. Hirasawa, M., Nakayama, M., Hase, T. & Knaff, D. B. Oxidation-reduction properties of maize ferredoxin: sulfite oxidoreductase. *Biochim. Biophys. Acta* **1608**, 140–148 (2004).
40. Bak, D. W. & Elliott, S. J. Alternative FeS cluster ligands: tuning redox potentials and chemistry. *Curr. Opin. Chem. Biol.* **19**, 50–58 (2014).
41. Lin, V. S., Lippert, A. R. & Chang, C. J. Cell-trappable fluorescent probes for endogenous hydrogen sulfide signaling and imaging H_2O_2-dependent H_2S production. *Proc. Natl Acad. Sci. USA* **110**, 7131–7135 (2013).
42. Navarro, F., Martín-Figueroa, E., Candau, P. & Florencio, F. J. Ferredoxin-dependent iron-sulfur flavoprotein glutamate synthase (GlsF) from the *Cyanobacterium synechocystis* sp. PCC 6803: expression and assembly in *Escherichia coli*. *Arch. Biochem. Biophys.* **379**, 267–276 (2000).
43. Mulholland, S. E., Gibney, B. R., Rabanal, F. & Dutton, L. P. Characterization of the fundamental protein ligand requirements of [4Fe-4S]$^{2+/+}$ clusters with sixteen amino acid maquettes. *J. Am. Chem. Soc.* **120**, 10296–10302 (1998).
44. Salis, H. M., Mirsky, E. A. & Voigt, C. A. Automated design of synthetic ribosome binding sites to control protein expression. *Nat. Biotechnol.* **27**, 946–950 (2009).

Acknowledgements

E. coli EW11 and the genes encoding *Zea mays* FNR, *Zea mays* SIR, and *Spinacia oleracea* Fd were a gift from P. Silver (Harvard University). Cellular assay development was supported by DOE grant DE-SC0014462 (G.N.B. and J.J.S.), split Fd efforts were supported by NASA grant NNX15AL28G (J.J.S. and G.N.B.), domain insertion efforts were supported by ONR grant N00014-17-1-2639 (J.J.S.), and electrochemistry was supported by DOE grant DE-SC0012598 (S.J.E.). J.T.A. was supported by NSF GRFP and DOE SGCSR fellowships.

Author contributions

J.T.A. designed and constructed all DNA vectors, performed the multiple sequence analysis, and did all cellular experiments. I.J.C. purified proteins and performed the lysate experiments. E.E.T. evaluated the switch substrate specificity profile. S.C.B. and S.J.E. performed the voltammetry. J.T.A., J.J.S., and G.N.B. conceptualized the project. J.T.A. and J.J.S. wrote the manuscript.

Competing interests

J.J.S., J.T.A., G.N.B., and I.J.C. have submitted a patent application (No 16/186,226) covering the use of fragmented Fds as chemical-dependent electron carriers, entitled "Regulating electron flow using fragmented proteins."

Additional information

Supplementary information is available for this paper at https://doi.org/10.1038/s41589-018-0192-3.

Reprints and permissions information is available at www.nature.com/reprints.

Correspondence and requests for materials should be addressed to J.J.S.

Publisher's note: Springer Nature remains neutral with regard to jurisdictional claims in published maps and institutional affiliations.

Methods

Materials. Rapamycin was from TCI America, isopropyl β-D-1-thiogalactopyranoside (IPTG) was from RPI, and all other chemicals were purchased from Sigma-Aldrich.

Vector design. Supplementary Table 1 lists all of the plasmids. These were constructed using Golden Gate DNA assembly[45] of PCR products amplified using Phusion DNA polymerase (Thermo Fisher). The genes encoding *Zea mays* FNR, *Z. mays* SIR, and *S. oleracea* Fd were a gift from P. Silver (Harvard University). The genes encoding *M. laminosus, Z. mays, C. reinhardtii,* and cyanomyophage PSSM-2 Fd were synthesized as G-blocks by Integrated DNA Technologies. The genes for *Ml*-Fd and sFd-35-ER were cloned into pET-28b to create expression vectors for protein purification. All vectors were sequence verified.

Calculations. A multiple sequence alignment (MSA) of 60 plant-type Fd sequences was generated using MUSCLE[5]. Positional amino acid sequence divergence was calculated as the number of unique amino acids observed at each *Ml*-Fd native site. Any site containing a gap in one or more Fd sequences was given a sequence divergence value of 20. The sequence divergence value for each Fd native site was calculated as the average for a sliding window of three sites. The UniProt numbers for each Fd are provided in Supplementary Fig. 1. The FASTA formatted MSA is included as Supplementary MSA.fasta and described in Supplementary Note 1.

Growth assay. For all growth experiments, *E. coli* EW11 were freshly transformed with two plasmids using electroporation, one encoding the electron donor and acceptor pair (FNR and SIR) and the other encoding either a native Fd, a C42A mutant of *Ml*-Fd that is unable to coordinate a [2Fe-2S] cluster, or an engineered Fd. Starter cultures were inoculated using single colonies obtained by selecting for colonies containing both plasmids on LB-agar plates. These starter cultures were grown in deep-well 96-well plates for 18 h at 37 °C in 1 mL of a nonselective modified M9 medium (M9c), which contained sodium phosphate, dibasic (6.8 g/L), sodium phosphate, monobasic (3 g/L), sodium chloride (0.5 g/L), 2% glucose, ammonium chloride (1 g/L), calcium chloride (0.1 mM), magnesium sulfate (10 mM), ferric citrate (24 mg/L), p-aminobenzoic acid (2 mg/L), inositol (20 mg/L), adenine (5 mg/L), uracil (20 mg/L), tryptophan (40 mg/L), tyrosine (1.2 mg/L), and the remaining 18 amino acids (80 mg/L each). For complementation analysis, starter cultures that had been grown to stationary phase in M9c were diluted ~1:100 using a 96-well replicator pin into 100 µL of a selective modified M9 medium (M9sa), which is identical to M9c but lacks cysteine and methionine. Cells were grown in the presence of the indicated amount of inducers (aTc, IPTG, rapamycin, or 4-HT) in an Infinite m1000 Pro plate reader (Tecan) at 37 °C with shaking at 250 r.p.m. at an amplitude of 1.5 mm in double-orbital mode. Optical density (OD) measurements were taken every 10 min. To select for the Fd and electron donor/acceptor plasmids, all growth steps included chloramphenicol and streptomycin at 34 µg/mL and 100 µg/mL, respectively.

Fluorescence spectroscopy. Whole-cell RFP measurements were done in the same way as the growth assay except starter cultures were diluted ~1:100 using a 96-well replicator pin into M9c medium (100 µL) and grown in an incubator at 37 °C with shaking at 250 r.p.m. After 24 h of growth, OD and fluorescence (λ_{ex} = 560 nm, λ_{em} = 650 nm) were measured using an Infinite m1000 Pro plate reader (Tecan). Fluorescence was normalized to OD and scaled relative to the condition without chemical inducer.

Protein purification. *E. coli* Rosetta transformed with pET28b containing the *Ml*-Fd or sFd-35-ER genes were grown at 37 °C in LB medium containing 50 µg/mL kanamycin to mid-log phase, induced using 50 µM IPTG, and grown overnight at 30 °C while shaking at 250 r.p.m. Cells harvested by centrifugation (4,000 *g*) were resuspended in 20 mL of lysis buffer (per L of culture) containing 10 mM Tris pH 8, 5 mM dithiothreitol (DTT), 10 mg/L DNase I, and 0.5 mg/mL lysozyme. After freezing overnight at −80 °C, cells were thawed and mixed with a cOmplete Mini, EDTA-Free protease inhibitor tablet (Sigma-Aldrich) at a ratio of one tablet per 400 mL of total cell lysate. Cell lysates were loaded onto a DE52 anion exchange column (Whatman) that had been equilibrated with TED buffer (25 mM Tris pH 8, 1 mM EDTA, and 1 mM DTT), the column was washed with TED containing 200 mM NaCl, and Fe-S proteins were eluted using TED containing 300 mM NaCl. The brown eluent was diluted with TED to bring NaCl below 100 mM and loaded onto HiTrap Q XL column (GE Healthcare) that had been equilibrated with TED using an AKTA Start FPLC system (GE Healthcare). This column was washed using TED buffer. A linear gradient was run from 0 to 375 mM NaCl TED and an isocratic 500 mM NaCl TED solution was used to elute the Fe-S proteins. SDS–PAGE was performed using NuPage 12% Bis–Tris Gels (Invitrogen) and the PageRuler Unstained Broad Range Protein Ladder (Thermo Scientific). Samples were concentrated 20-fold using an Amicon Ultra 10 K MWCO spin column. Concentrated samples were flash frozen with liquid nitrogen.

Spectroscopy. Purified *Ml*-Fd and sFd-35-ER were dialyzed into TED buffer (25 mM Tris pH 8, 1 mM EDTA, 1 mM DTT). Each protein was incubated with 4-HT (100 µM) or the carrier DMSO used to dissolve 4-HT (1% of final volume) for 30 min. A J-815 spectropolarimeter (Jasco) was used to measure the ellipticity of samples from 700 nm to 300 nm. UV/Vis absorbance of samples was read using a Cary 50 UV-Vis Spectrophotometer (Varian) from 600 nm to 250 nm. Measurements used quartz cuvettes with a 1-cm path length. Experiments performed twice using two distinct protein preparations yielded the same result.

Cell lysates. Electrocompetent *E. coli* EW11 were transformed with the plasmid (pSAC01) that constitutively expresses *Z. mays* FNR and SIR. Cells were grown to stationary phase at 37 °C and 250 r.p.m. in 2xYTPG medium (16 g/L tryptone, 10 g/L yeast extract, 5 g/L NaCl, 3 g/L KH_2PO_4, 7 g/L K_2HPO_4, and 18 g/L glucose) containing 100 µg/mL streptomycin. Cells from overnight cultures were diluted 1:100 in fresh 2xYTPG medium containing streptomycin, grown for 2 h at 37 °C while shaking at 250 r.p.m. until mid-log phase, and then shifted to 30 °C and grown for an additional 4 h. Cell cultures were harvested by centrifugation (4,000 *g*), and cells were resuspended in equal volume of S30 buffer (10 mM Tris-acetate, 14 mM magnesium acetate, 60 mM potassium acetate pH 8.2) and washed twice with S30 buffer; the pellets were weighed and flash frozen with liquid nitrogen. Pellets were thawed, resuspended in 2 mL of S30 buffer per gram of cell pellet, and sonicated using a Q500 Sonicator (Qsonica) with the probe at 20 kHz and 40% maximal amplitude until samples had been exposed to ~0.5 Joules of sonication energy per microliter of cell slurry[36]. To minimize sample overheating, sonication proceeded for 25 s followed by a 15 s rest period between sonication pulses. To remove native reduced cofactors like NADH and NADPH, lysates were applied to a Zeba Spin Desalting Column 7 K MWCO (Thermo Scientific) that had been equilibrated with S30 buffer. Protein content in lysates was quantified using Bio-Rad Protein Assay Dye Reagent Concentrate (Bio-Rad), using bovine serum albumin (NEB) as a standard.

Sulfide production assay. To visualize sulfide production, we diluted cells lysates two-fold into S30 buffer to 4.8 mg/mL of total protein. Desalted lysates were diluted 1.25-fold with 5× LSR buffer, which contained 50 mM sodium sulfite, 200 µM β-nicotinamide adenine dinucleotide 2′-phosphate reduced tetrasodium salt (NADPH), 10 µM sulfidefluor 7 AM (Tocris)[26], 670 mM potassium acetate, 50 mM ammonium acetate, 40 mM magnesium acetate, and 50 mM potassium phosphate, dibasic pH 7.2. To analyze background sulfide production from lysates alone, we added additional NADPH to the lysate/LSR mixture to achieve higher concentrations. To analyze we added Fd-dependent sulfide production, purified *Ml*-Fd or sFd-35-ER at the indicated concentrations to the lysate diluent S30 buffer. To limit disulfide bond formation in the ER-LBD sFd-35-ER, which has been observed in past studies[42], we first reduced this protein with freshly made 1 mM DTT in S30 buffer for 20 min on ice and then desalted immediately before addition to the assay using a Zeba Spin Desalting Columns, 7 K MWCO. Following NADPH or protein addition, reactions were arrayed in a Corning 96 well plate at room temperature (Costar #3603), transferred to an Infinite m1000 Pro plate reader (Tecan), heated to 37 °C, and shaken at 250 r.p.m. with fluorescence readings (λ_{ex} = 495 nm, λ_{em} = 520 nm) every 15 s. When analyzing chemical-dependent sulfide production, 12.5 µM 4-hdyroxytamoxifen (4HT) or blank ethanol was injected into the plate following two minutes of incubation and the lysate diluent S30 buffer volume was reduced accordingly.

Midpoint potentials. Electrochemical experiments were carried out anaerobically in a MBraun Labmaster glovebox using a PGSTAT12 potentiostat. A three-electrode configuration was used in a water-jacketed glass cell. A platinum wire was used as the counter electrode, and a standard calomel electrode was used as the reference electrode. Reported potentials are relative to the standard hydrogen electrode. Baseline measurements were collected using an edge-plane graphite (EPG) electrode that was modified with a 100 mM neomycin trisulfate solution, rinsed, and placed into a glass cell containing a 23.5 °C mixed buffer solution (5 mM acetate/MES/MOPS/TAPS/CHES/CAPS) pH 7.0, with 100 mM NaCl. A 5-µL aliquot of 720 µM *Ml*-Fd or 5 mM sFd-35-ER was applied directly to the electrode surface with or without 1 µL of 50 mM 4-HT, and the protein was allowed to reduce in size for approximately 1 min at room temperature before being placed into the buffer cell solution. Square wave voltammograms were collected at 23.5 °C with a frequency of 10 Hz, and electrochemical signals were analyzed using QSoas. Experiments performed twice using two distinct protein preparations yielded the same result.

Statistical analysis. Growth assays and whole-cell fluorescence data are reported as the mean and s.d. of biologically independent samples (n = 3). The sulfide production data are reported as the mean and s.d. of independent experiments (n = 3). All reported P values were obtained using two-tailed, independent t-tests. Sample sizes were in accordance with community standards.

Reporting Summary. Further information on research design is available in the Nature Research Reporting Summary linked to this article.

Data availability

There are no restrictions on data availability. Accession codes and sequences used for multiple sequence alignments are provided in Supplementary Note 1. Raw data for Figs. 1, 2 and 3 are available upon request.

References

45. Engler, C., Kandzia, R. & Marillonnet, S. A one pot, one step, precision cloning method with high throughput capability. *PLoS One* **3**, e3647 (2008).

nature research

Corresponding author(s): Jonathan Silberg

Reporting Summary

Nature Research wishes to improve the reproducibility of the work that we publish. This form provides structure for consistency and transparency in reporting. For further information on Nature Research policies, see Authors & Referees and the Editorial Policy Checklist.

Statistical parameters

When statistical analyses are reported, confirm that the following items are present in the relevant location (e.g. figure legend, table legend, main text, or Methods section).

n/a	Confirmed	
☐	☒	The exact sample size (*n*) for each experimental group/condition, given as a discrete number and unit of measurement
☐	☒	An indication of whether measurements were taken from distinct samples or whether the same sample was measured repeatedly
☐	☒	The statistical test(s) used AND whether they are one- or two-sided *Only common tests should be described solely by name; describe more complex techniques in the Methods section.*
☒	☐	A description of all covariates tested
☐	☒	A description of any assumptions or corrections, such as tests of normality and adjustment for multiple comparisons
☐	☒	A full description of the statistics including central tendency (e.g. means) or other basic estimates (e.g. regression coefficient) AND variation (e.g. standard deviation) or associated estimates of uncertainty (e.g. confidence intervals)
☒	☐	For null hypothesis testing, the test statistic (e.g. *F*, *t*, *r*) with confidence intervals, effect sizes, degrees of freedom and *P* value noted *Give P values as exact values whenever suitable.*
☒	☐	For Bayesian analysis, information on the choice of priors and Markov chain Monte Carlo settings
☒	☐	For hierarchical and complex designs, identification of the appropriate level for tests and full reporting of outcomes
☒	☐	Estimates of effect sizes (e.g. Cohen's *d*, Pearson's *r*), indicating how they were calculated
☐	☒	Clearly defined error bars *State explicitly what error bars represent (e.g. SD, SE, CI)*

Our web collection on statistics for biologists may be useful.

Software and code

Policy information about availability of computer code

Data collection	Growth and fluorescence data were collected using Tecan i-Control v3.7.3 Absorbance and circular dichroism data were collected using Spectra Manager 2 Protein film voltammetry data were collected using General Purpose Electrochemical System (GPES) version 4.9
Data analysis	Microsoft Excel 16 for Windows Python (numpy, scipy, matplotlib) Previously published MUSCLE and MATT sequence/structure alignment algorithms QSoas

For manuscripts utilizing custom algorithms or software that are central to the research but not yet described in published literature, software must be made available to editors/reviewers upon request. We strongly encourage code deposition in a community repository (e.g. GitHub). See the Nature Research guidelines for submitting code & software for further information.

Data

Policy information about availability of data

All manuscripts must include a data availability statement. This statement should provide the following information, where applicable:

- Accession codes, unique identifiers, or web links for publicly available datasets
- A list of figures that have associated raw data
- A description of any restrictions on data availability

There are no restrictions on data availability. Accession codes and sequences used for multiple sequence alignments are provided in the supplement. Raw data for Figures 1-4 are available upon request

Field-specific reporting

Please select the best fit for your research. If you are not sure, read the appropriate sections before making your selection.

☒ Life sciences ☐ Behavioural & social sciences ☐ Ecological, evolutionary & environmental sciences

For a reference copy of the document with all sections, see nature.com/authors/policies/ReportingSummary-flat.pdf

Life sciences study design

All studies must disclose on these points even when the disclosure is negative.

Sample size	Sample sizes were chosen in accordance with community standards all experiments were performed in triplicate (n=3) except for protein spectroscopy and voltammetry which were performed twice on unique protein preparations each yielding identical results which exceeds community standards.
Data exclusions	No data were excluded from analyses
Replication	All replication attempts in this study were successful
Randomization	All bacterial cell cultures used for each experiments were grown under the same conditions, so randomization was not relevant
Blinding	This study only provides objective measurements of samples derived from bacterial cultures subjected to identical growth conditions per experiment. Blinding was not relevant for this study

Reporting for specific materials, systems and methods

Materials & experimental systems

n/a	Involved in the study
☐	☒ Unique biological materials
☒	☐ Antibodies
☒	☐ Eukaryotic cell lines
☒	☐ Palaeontology
☒	☐ Animals and other organisms
☒	☐ Human research participants

Methods

n/a	Involved in the study
☒	☐ ChIP-seq
☒	☐ Flow cytometry
☒	☐ MRI-based neuroimaging

Unique biological materials

Policy information about availability of materials

Obtaining unique materials	No restrictions on availability apply. All plasmids will be available on Addgene